Journal of Computer-Aided Molecular Design, **16:** 769–778, 2002.
KLUWER/ESCOM

Binding models of reversible inhibitors to type-B monoamine oxidase

Antonio Carrieri[a,*], Andrea Carotti[a], M. Letizia Barreca[b] & Cosimo Altomare[a]
[a]*Dipartimento Farmaco-Chimico, Università di Bari, Via Orabona 4, 70125 Bari, Italy,* [b]*Dipartimento Farmaco-Chimico, Università di Messina, Viale SS. Annunziata, 98168 Messina, Italy*

Received 10 October 2002; Accepted 6 January 2003

Key words: Monoamine oxidase-B, reversible MAO-B inhibitors, three-dimensional quantitative structure-activity relationships, docking calculations

Summary

Interest in the inhibitors of type-B monoamine oxidase has grown in recent years, due to the evidence for multiple roles of one such agent (selegiline) in the pharmacological management of neurodegenerative disorders. A set of 130 reversible and selective inhibitors of MAO-B (including tetrazole, oxadiazolone, and oxadiazinone derivatives) were taken from the literature and subjected to a three-dimensional quantitative structure–activity relationship (3D-QSAR) study, using CoMFA and GOLPE procedures. The steric and lipophilic fields, alone and in combination, provided us with informative models and satisfactory predictions ($q^2 = 0.73$). The validity of these models was checked against the 3D X-ray structure of human MAO-B. Flexible docking calculations, performed by using a new approach which took advantage from QXP and GRID computational tools, showed the diverse inhibitors to interact with MAO-B in a similar binding mode, irrespective of the heterocycle characterizing them. A significant trend of correlation was observed between estimated energies of the complexes and the experimental inhibition data.

Introduction

Monoamine oxidase (MAO, EC 1.4.3.4) is a flavin-dependent enzyme tightly bound to the mitochondrial outer membranes of neuronal, glial, and other cells. It plays a major role in the oxidative deamination of biogenic (neurotransmitters) and diet-derived amines in both the central nervous system (CNS) and in peripheral neurons and tissues [1]. Two isozymes of MAO (A and B) have been distinguished on the basis of their substrate preference and inhibitor selectivity. MAO-A preferentially deaminates serotonin, norepinephrine and epinephrine (it catalyzes the oxidation of food tyramine in the intestine), and is selectively and irreversibly inhibited by clorgyline (**1**, Figure 1). MAO-B preferentially deaminates β-phenylethylamine and benzylamine, and is irreversibly inhibited by pargyline **2** and selegiline **3** (i.e., *L*-deprenyl) [2]. MAO-A and B have different histological localizations [3], and a molecular basis for differences in enzymatic properties has been provided by cDNA cloning [4] and site-directed mutagenesis data [5]. They are coded for by separate but closely related genes on the X chromosome [6] and share a 70% sequence identity [7], whereas differ by their binding sites and possibly by their lipid environment [8–10].

MAO-A inhibitors (Is) have found application in the treatment of depression, and MAO-B Is in the pharmacological management of Parkinson's disease [11]. Due to the evidence of a neuroprotective effect of selegiline (the first selective MAO-B inhibitor identified, lacking of the so-called 'cheese effect') [12], MAO-B Is have become attractive neuropharmacological agents. The multiple roles of MAO-B Is in the therapy of neurodegenerative disorders, including the Alzheimer's disease, have been extensively reviewed [13]. The majority of currently investigated MAO-B Is are irreversible. There are fewer specific reversible inhibitors of MAO-B (e.g., lazabemide **4**) with respect to MAO-A. Hence, the development of selective and

*To whom correspondence should be addressed. E-mail: carrieri@farmchim.uniba.it

reversible inhibitors of MAOs, potentially devoid of the undesirable side-effects associated to the old irreversible MAO Is, still remains a major task which could helpfully profit from the computational tools of drug design.

Though several ligand-based models, including 3D-QSARs developed by some of us [14–16], have been reported for several classes of MAO Is, the molecular requirements responsible for selective inhibition are far from being fully understood. The crystal structure of human MAO-B has been very recently elucidated [17], so providing relevant information for the design of selective inhibitors.

With the aim of highlighting the molecular factors responsible for MAO I activity and selectivity, we undertook a computational study of diverse MAO reversible inhibitors. Herein we report on the molecular modeling of reversible inhibitors, acting preferentially on MAO-B, a part of them being taken from literature (e.g., tetrazoles **5**, oxadiazolones **6**, oxadiazinones **7**, and aryl N-acylhydrazones **8**) [18–22], the other being chosen among the inhibitors recently developed by us (e.g., condensed diazines, such as cmpd **9** [14] in Figure 1, and coumarin derivatives, such as cmpds **10** and **11** [16]). The results from a CoMFA-based 3D-QSAR study of a large set of known MAO-B reversible inhibitors are here reported and compared with models of binding to human MAO-B generated through flexible docking calculations, by using a new approach that takes advantage from QXP [23] and GRID [24] computational tools.

Computational methods

CoMFA (3D-QSAR) study

Molecular models of the analyzed MAO-B Is were built using standard bond distances and angles of SYBYL (Ver. 6.8) software (Tripos Assoc. St. Louis, MO, U.S.A). Full geometry optimization was performed with the AM1 Hamiltonian using the parameter set reported in the MOPAC (ver. 6.0) suite of programs [25]. In the CoMFA studies, electrostatic potentials (MEPs) were calculated using Mulliken atomic charges from AM1 calculations for allowing our 3D-QSAR results to be compared with those from *ab initio* calculations published a number of years ago by Wouters and colleagues [26] on similar datasets. Indeed, MEPs based on AM1 wave functions, which provide a good compromise between the accuracy of the results and the computer time expense, correlate quite well with *ab initio* results [27].

In order to generate a suitable alignment for the selected compounds, the flexible template fitting module TFIT implemented in QXP [23] was used. 100 runs of Monte Carlo followed by conjugate gradient minimization were performed, resulting then in a low energy conformation for each ligand having an extended geometry.

3D-QSAR was carried out by calculating the steric and electrostatic fields by SYBYL and molecular lipophilicity potential (MLP) [28] by CLIP 1.0 (Institute of Medicinal Chemistry, University of Lausanne, Lausanne, Switzerland). CoMFA [29] setup previously described was applied [16]. The GOLPE 4.5 software (Multivariate Infometric Analysis, Perugia, Italy) was used to perform variable selection and to validate and interpret the models [30]. The steric, electrostatic and lipophilic fields were exported to GOLPE where the field matrix was unfolded to produce one-dimensional vector variables for each compound. The original matrix with field values (4,227 variables) was then pretreated in order to select unbiased variables by zeroing the positive and negative ones up to 0.17 kcal/mol, and applying a standard deviation cutoff up to 0.22 kcal/mol. The smart region definition (SRD) algorithm was used with the default setting in order to group chemometrically and three-dimensionally close variables, followed by three consecutive FFD variables selection runs. The number of variables retained after variable selection are reported in Table 1.

PLS crossvalidation analyses were performed adopting the 'leave-one-out' mode. In all cases, the number of PLS components to be used in generating the final 3D-QSARs (i.e., Optimal Number of Components, ONC) was taken as the number of latent variables beyond which further addition of components did not increase the crossvalidation coefficient (q^2) by at least 0.05.

QX-GRID

For human MAO B structure, chain A of the X-ray crystallographic structure (PDB code 1gos) was used. After the removal of the covalently bound pargyline from the complex, polar hydrogens were added and the structure was then minimized within MACROMODEL ver. 7.0 (Schrödinger, Portland, OR, USA) in three steps: 5000 iterations of steepest descent were carried out keeping fixed the Cα trace of the protein

(a) irreversible, selective

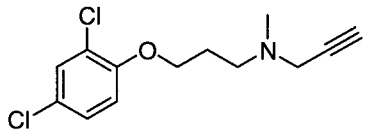

1 (MAO-A)

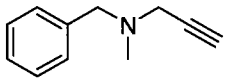

2 (MAO-B)

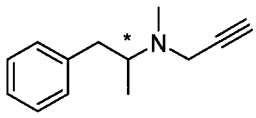

3 (MAO-B)

(b) reversible, MAO-B selective

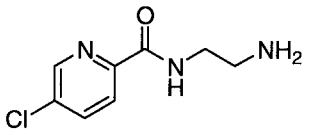

4

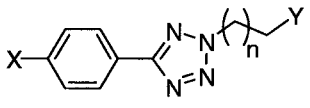

5

n = 1 – 5
X = H, Cl, NO_2, OMe, Ph, $OCH_2C_6H_4$-X';
Y = OH, CN

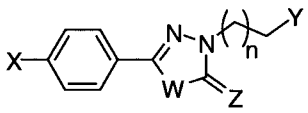

6

n = 0 – 3
W and/or Z = O, S; X = H, Me, Cl, NO_2, OMe, Ph, $OCH_2C_6H_4$-X'
Y = OH, CN

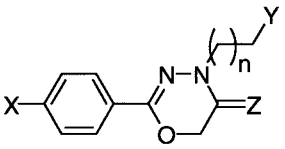

7

n = 0 – 3
X = H, NO_2, OMe, Ph, $OCH_2C_6H_4$-X'
Y = H, Br, OH, OMe, COOMe, CN
Z = O, S

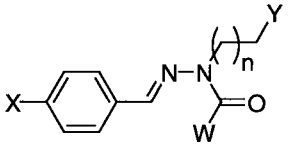

8

n = 0, 1
X = H, $OCH_2C_6H_4$-X'
Y = OH, COOMe, CN
W = Me, OEt, NHMe

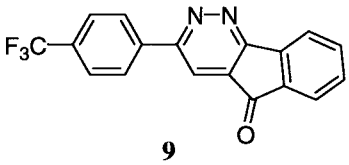

9

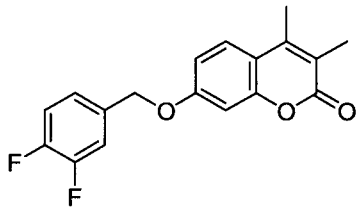

10

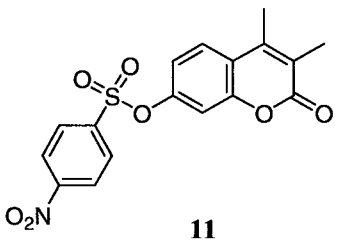

11

Figure 1. Structures of known irreversible (a) and reversible (b) inhibitors of MAOs. The sets of compounds numbered as **5-8** have been used in the 3D-QSAR study.

followed by 5000 runs of conjugate gradient where the only α-helices and β-sheets were constrained; finally, the whole structure was relaxed until the RMS gradient was less then 0.001 kcal/mol Å. The AMBER* force field [31] and the solvent continuum method were applied.

The ligand docking studies were performed using an approach integrating QXP and GRID computational tools (hereafter called QX-GRID). The subsequential steps of the methodology used are illustrated in Figure 2. QX-GRID takes advantages from energetically favorable MIPs calculated on the target protein as guide atoms for a template fitting procedure, where a molecule is rotated and translated in the 3D space, in order to search for the best superposition between atoms in the ligand and similar atom types having the cartesian coordinates corresponding to the previously computed MIPs. In this step, the optimal overlap between atoms is carried out by minimizing the superposition energy term implemented in the force field of the QXP software (ver. 98). At the same time, not only the cartesian coordinates but also the internal geometry (i.e., dihedral angles) of the molecule are perturbed according to the classical Metropolis Monte Carlo algorithm, in order to obtain low energy molecule conformations. Each possible solution detected by the fitting algorithm is in turn transferred, once again, to GRID, where the MIP with the target are calculated, this time using not atoms but the whole molecule as a probe. A binding energy (BE) is finally calculated using the GRID force field. The energy terms describing this scoring function are enthalpy- and entropy-related contributions to the ligand-target interactions: three terms (ligand-target enthalpic interaction energy, water bridges between ligand and target, and a term contributed by hydrophobic interactions) favor ligand binding, whereas four penalty terms (for displacing pre-bound waters from target and from ligand, for mutually incompatible water molecules, and for restricted rotational torsions) tend to oppose it.

One of the main rewards of the latest step is that the positions of water molecules potentially solvating the target and the ligand are also calculated. Hence, favorable contribution of additional H-bonds in stabilizing the binding to the enzyme are also taken into account.

In our case, the MIPs were calculated on the fully minimized MAO-B structure, using a $61 \times 61 \times 61$ cubic cage (grid spacing $= 0.5$ Å) centred on the cartesian coordinates of the core of the covalently linked pargyline. A number of suitable atom probes were chosen according to the nature (type, hybridization, charge, etc.) of heteroatoms present in each ligand to be docked, whereas for carbon atoms the hydrophobic DRY probe was selected.

For the template fitting procedure, 1000 runs of Monte Carlo were performed by means of the TFIT-DYN module of QXP; at each run a Polack-Ribiere conjugate gradient minimization is performed. The best 100 energy solutions within an energy threshold of 25 kcal/mol were stored. In the BE calculation for these conformers, the directives FOBE, WATA, WENT and TORS were set at the default values of 5, -5, -1 and 0, respectively (for the meaning of these directives see the GRID manual available on line at <http://www.moldiscovery.com>). In order to take into account the flexibility of protein side chains the directive MOVE was set to 1.

Calculations were run on either one of SGI Origin300 R14000, SGI O2 R10000 and SGI230 PIII 1Ghz workstations.

Results and discussion

3D-QSARs of diazoheterocycle-containing inhibitors of MAO-B

Inhibition data for more than one hundred heterocyclic compounds, including 35 tetrazoles **5** [18], 41 oxadiazolones **6** [19, 20], 34 oxadiazinones **7** [21], were selected from the available literature according to predefined criteria, namely homogeneity of enzyme sources and biochemical assay. They contain as a common characteristic the 'diazo' N-N moiety (Figure 1), and are mostly potent and selective reversible inhibitors of type B of MAO. A general look at the SARs revealed a major role of the terminal benzyloxy moiety, and the lipophilicity as the parameter mainly governing the inhibition activity irrespective of the nature of the heterocycle. In fact, opening the oxadiazolone ring provided a set of N-acylhydrazone derivatives **8** (Figure 1), which still retained MAO-B inhibition activity [22]. A set of 22 compounds **8** was also included in the 3D-QSAR study.

Actually, based on theoretical studies (*ab initio* calculations), Wouters and colleagues in 1997 [26] proposed a qualitative model of SARs that highlighted physicochemical factors essential for MAO-B reversible inhibition: (i) a planar aryl diazoheterocyclic support showing a conserved pattern of H-bond acceptor sites; (ii) a lateral ethyl chain bearing a CN

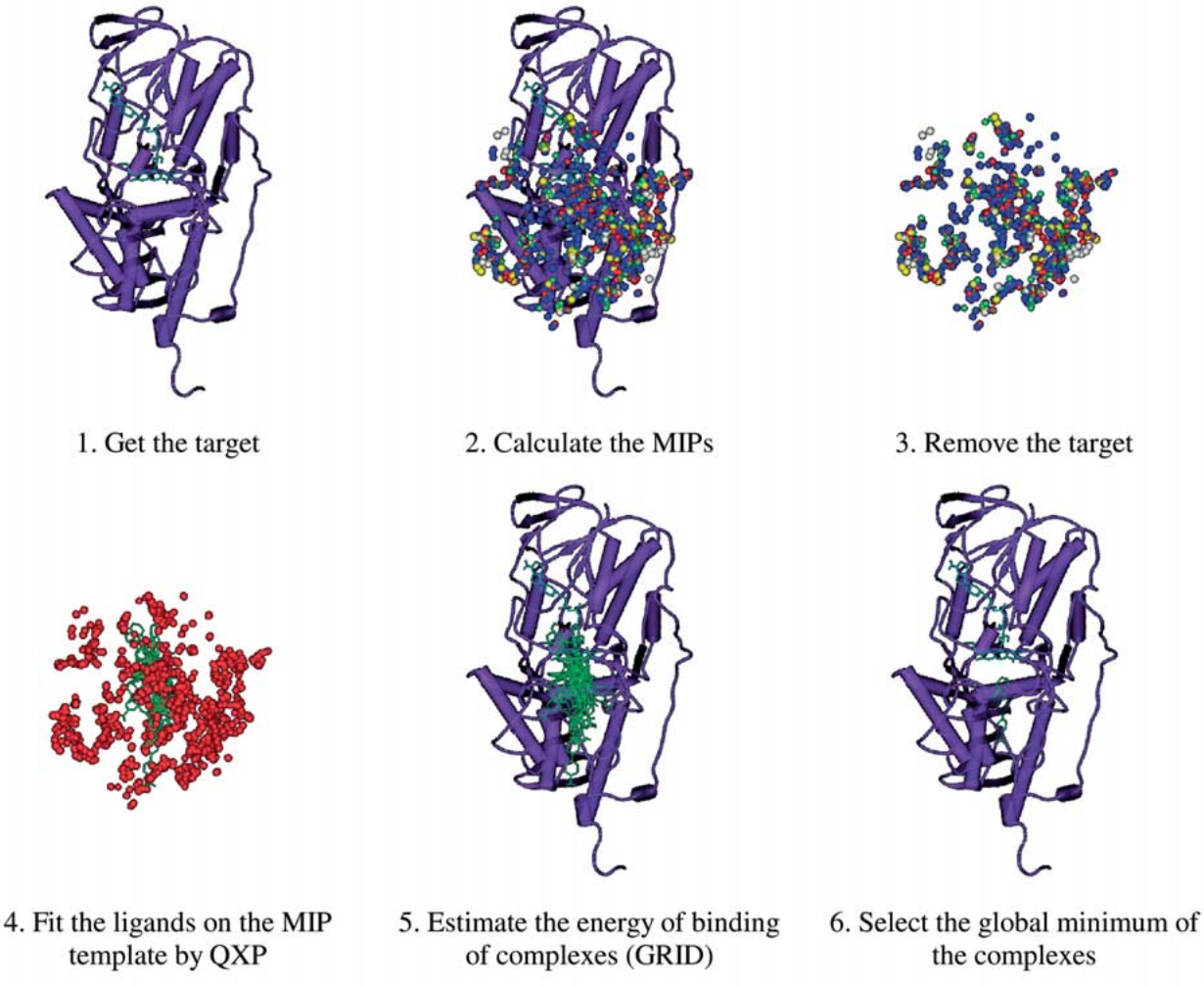

Figure 2. QX-GRID methodology breakdown.

or OR terminal group able to reach the catalytic site of the enzyme without reacting with it; (iii) a hydrophobic tail (the benzyloxy chain) interacting with a hydrophobic binding site of the protein.

To prove these SARs on a more quantitative basis, we performed a 3D-QSAR study, using CoMFA with standard steric and electrostatic fields, and molecular lipophilicity potential (MLP), which in our previous studies on other sets of MAO-B reversible Is had been found to significantly improve the correlative, predictive, and interpretative power of CoMFAs [14, 16]. Steric (*ste*) and electrostatic (*ele*) fields, and MLP (*lip*) were calculated, and the matrix of 3D descriptors generated in SYBYL (CoMFA columns) was exported in GOLPE to be subjected to a pretreatment aimed at retaining only the informative variables. 3D-QSARs for individual molecular sets resulted in satisfactory one-field models (results not shown). With the exception of the aryl N-acylhydrazone set, the steric 3D descriptors were found as the most explanatory and predictive variables. In the CoMFA model for the oxadiazolones two outliers, bearing as unique structural variations, ramifications on the lateral N(3)-chain (i.e., 2-cyanopropyl and 3-cyanobutyl instead of the most common 2-cyanoethyl chain), were found and omitted from the subsequent analyses. The four sets of MAO-B Is **5**-**8** were then combined to yield good models for 130 compounds. The statistics of CoMFA/GOLPE models in Table 1 proved the MAO-B inhibition activity to depend mainly upon favorable and unfavorable steric interactions.

Table 1. Statistics of the CoMFA/GOLPE models on diazoheterocycle-containing MAO-B inhibitors (130 compounds)

Model	Field type	Var[a]	q^{2b}	r^{2c}	SDEP[d]
B1	ste	312	0.72	0.79	0.70
B2	ele	300	0.30	0.39	1.11
B3	lip	254	0.67	0.74	0.76
B4	ste and ele	305	0.72	0.79	0.70
B5	ste and lip	341	0.73	0.79	0.69
B6	ele and lip	322	0.68	0.74	0.75
B7	ste, ele, and lip	314	0.73	0.80	0.69

[a]Number of variables retained after pretreatment.
[b]Squared cross-validated correlation coefficient (optimal number of PLS components = 4).
[c]Squared correlation coefficient.
[d]Standard Deviation of Error of Predictions.

Figure 3. PLS coefficient contour maps for the CoMFA/GOLPE model **B5** of the MAO-B Is (*ste* contour levels: 0.025 green and −0.002 red; *lip* contour levels: 0.004 yellow and −0.004 cyan). The most active compounds (pIC_{50} 8.70-8.10) are displayed to aid interpretation.

MLP alone gave also a model of interest. Combining the *ste* variables with the *ele* or *lip* ones did not result in strong improvements of the statistics. We developed the model incorporating *ste* and *lip* fields (model **B5**), rather than for statistical reasons (a slight increase of q^2 was however attained), because it allowed us a better interpretation of the binding mode.

As shown by the coefficient contour maps of the two-field model **B5**, displayed in Figure 3, a large green-colored region (more or less coincident with the yellow region in the *lip* contours) indicates that the inhibition activity mainly increases due to hydrophobic interactions of the benzyloxy moiety. A large red zone close to the N(3) lateral chain (the 2-cyanoethyl chain has the optimal length) accounts for a steric hindrance resulting from its elongation. Two cyan regions appeared in the *lip* contour map, which indicate unfavorable hydrophobic interactions, or alternatively H-bond and polar interactions favoring the binding, close to the diazoheterocyclic moiety and to the *para* position of the phenyl ring in the benzyloxy tail. Apparently, the former highlights the importance of a given pattern of H-bond acceptor sites on the diazoheterocycle moiety. In contrast, the second cyan polyhedron, rather than indicating favorable polar and/or H-bond interactions, should result from the fact that any substituent in *para* (but also *meta*) position, even if lipophilic, did not at all contribute to increase the MAO-B inhibitory activity, as the biological data proved. Such a PLS/CoMFA result seems like a translation in 3D QSAR terms of a nonlinear (parabolic or bilinear) relationship between activity and lipophilicity.

The 3D-QSAR models, providing quantitative support to the SARs of Wouters *et al.* [26], agree quite well with those previously obtained by some of us with other classes of MAO reversible inhibitors. The influence of lipophilicity in increasing inhibition of MAO-B (but not MAO-A) had been indeed demonstrated by a QSAR Hansch-type analysis and by CoMFA incorporating the MLP, either for 3-substituted-5*H*-indeno[1,2-*c*]pyridazin-5-ones [14] (the structure of the most active inhibitor **9**, is reported in Figure 1) and for 7-X-substituted benzyloxy-3,4-dimethylcoumarins [16] (cmpd **10** was the most active one). 3D-QSARs pointed out especially the role of hydrophobic interactions of the benzyloxy chain in diazoheterocycle-containing inhibitors and in our coumarin derivatives, or *para*-trifluoromethylphenyl in our indenopyridazine compounds. What is the site of such a hydrophobic interaction that significantly contribute to increase the inhibitory activity of MAO-B by diverse compounds is a major point that deserved a deeper investigation.

The X-ray crystallographic structure of human MAO-B has been very recently determined to 3 Å resolution [17]. The active site consists in a 420 $Å^3$-hydrophobic cavity, lined by a number of aromatic and aliphatic amino acids, interconnected to an entrance cavity of 290 $Å^3$. Residues Tyr326, Ile199, Leu171 and Phe168 are the side chains which separate the two cavities, and the recognition site for the substrates is a cage-like region lined by Tyr398 and Tyr435 and

Table 2. Inhibition activity as predicted by 3D-QSAR models and binding energies (BE) calculated on the enzyme-inhibitor complexes as found by QX-GRID method.

Cmpd[a]	X	pIC_{50}		BE
		obs	pred[c]	(kcal/mol)
5a	NO_2	4.87	4.51	−9.39
5b	OCH_3	4.43	4.63	−2.78
5c	C_6H_5	6.08	5.77	−7.13
5d	OCH_2–*p*-FC_6H_4	6.68	6.90	−8.70
5e	OCH_2–*p*-$CH_3C_6H_4$	6.24	5.95	−5.63
5f	$OCH_2C_6H_5$	8.70	6.89	−10.22
6a	CH_3	3.89	5.35	−4.39
6b[b]	OCH_3	5.39	4.70	−10.12
6c	$OCH_2C_6H_5$	8.66	7.76	−11.13
6d[b]	OCH_2–*p*-$OCH_3C_6H_4$	6.04	6.64	−6.61
7a	H	4.25	4.30	−2.79
7b	$OCH_2C_6H_5$	7.74	7.05	−9.89
8a	H (W=CH_3)	3.40	4.49	−5.68
8b	$OCH_2C_6H_5$ (W=OC_2H_5)	5.20	5.82	−8.02
8c	$OCH_2C_6H_5$ (W=CH_3)	8.52	6.91	−12.03

[a]Structures in Figure 1.
[b]Z=S instead of O as in all the other compounds.
[c]Activity values predicted by 3D-QSAR model **B5** during cross-validation procedure.

the isoalloxazine ring of the flavin cofactor at the top (for a picture of the two cavities, with the residues lining them differently colored and the hydrophobic interactions taking place inside highlighted by favorable MIPs calculated with the DRY probe of GRID, see below Figure 4a).

A structure-based interpretation of the selectivity of MAO inhibitors toward A and B isoenzymes can not leave out of consideration the important information obtained from mutagenesis data. A critical mutation was that of Tyr326 into the corresponding residue of MAO A (Ile335) which inverted the selective binding of MAO Is [5].

The detection of an entrance cavity connecting the surface of the protein to the substrate cavity in MAO-B brought us to formulate the hypothesis that such a cavity may be an additional site for stabilizing the binding of reversible inhibitors. In order to possibly gain proofs supporting this hypothesis, we performed docking calculations using the X-ray structure of human MAO-B as the enzyme target and a number of reversible inhibitors chosen among those used in the 3D-QSAR studies.

Docking of reversible MAO-B Is

Automated docking algorithms have demonstrate great utility in assisting drug design processes. Nevertheless, efforts are still required in order to develop suitable scoring functions for binding energies able to correctly rank ligands according to their biological activity [32]. Several docking calculation methods are available (for a comprehensive review see [33]), but not all are capable to reliably account for all the intertwining events that underlay the recognition between a ligand and a receptor, such as the mutual dynamic adaptability (e.g., protein/ligand flexibility) and the role of the water molecules. We believe that the generation of hypotheses of ligand binding mode through docking calculations can somehow take advantage from a careful consideration of the 3D-QSAR ligand-based models. This seems the case of diazoheterocyclic MAO-B inhibitors under our examination.

Fifteen compounds, including weak, moderate and strong inhibitors, were selected among those previously used in the 3D-QSAR analysis (see Figure 1 for structures and Table 2 for the biological data) and subjected to flexible docking calculations, using the X-ray structure of MAO-B as the receptor. The above described QX-GRID approach was used in order to generate a hypothesis of binding mode of diazoheterocylic MAO-B inhibitors (computational details in the methodological section and Figure 2).

In Figure 4b the docking model generated through our QX-GRID calculations for the most active inhibitor within the whole series examined, i.e., 3-{5-[4-(benzyloxy)phenyl]-2*H*-tetrazol-2-yl}propanenitrile (**5f**, Table 2), is shown. The most stable enzyme-inhibitor complex found by our method detected the substrate cavity and the interconnected entrance cavity (Phe103, Trp119, Leu164, and Phe168, which are among the residues lining such a cavity, are highlighted in the figure) as the enzyme sites involved in the binding of the tetrazole-containing reversible inhibitor. Tyr326 appears to be involved in an edge-to-face aromatic interaction with the central phenyl ring of the inhibitor. The hydrophobic tail, i.e., the benzyloxy group, is embedded into the entrance cavity. This finding, in agreement with the 3D-QSAR model, suggests that such a hydrophobic cavity may represent a relevant binding site to be taken into account in the design of MAO-B reversible inhibitors. In addition, QX-GRID led us to identify where water molecules might be properly located in

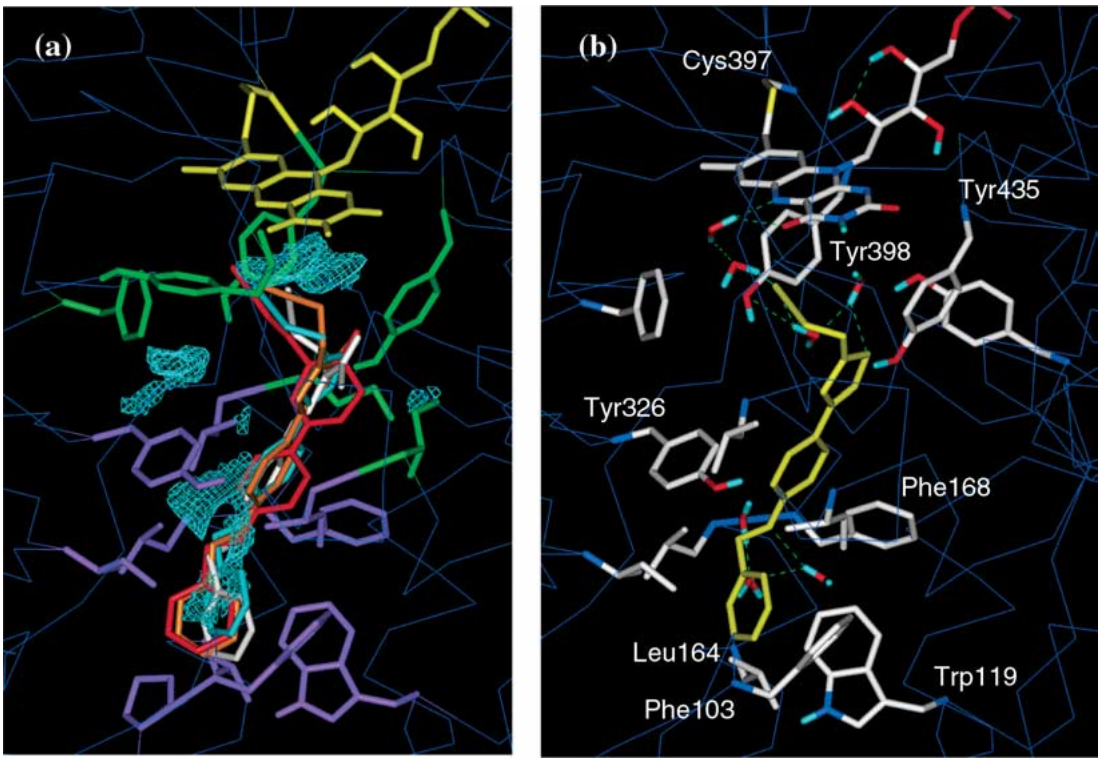

Figure 4. (a) Enzyme-ligand complex for cmpds **5f** (cyan), **6b** (orange), **7c** (red) and **8c** (white); the hydrophobic MIPs, calculated using the DRY probe (contour level -1 kcal/mol), are represented as cyan meshed surface. The FAD moiety, residues lining the substrate cavity and the entrance cavity of the enzyme are colored in yellow, green and violet, respectively. (b) Results from docking calculations performed by our QX-GRID approach on reversible MAO-B Is: cmpd **5f** docked into the binding site of the enzyme; the most relevant residues lining the substrate site and the entrance cavity, and water molecules stabilizing the complex, are displayed.

order to promote the binding of the ligand. As it can be observed in Figure 4b, more then one water molecules seem to trap the ligand through a H-bonding network involving the flavin ring and Tyr398 within the substrate cavity, and the polar atoms or groups in the tetrazole moiety of the inhibitor. Interestingly, irrespective of the diazoheterocycle characterizing the molecules under examination, the QX-GRID method found a quite close binding mode for all the ligands (Figure 4a).

Finally, we wanted to check whether the proposed method is also able to rank the different inhibitors with respect to their measured inhibitory activity. As a matter of fact, a trend of correlation was observed between the estimated binding energy values (BEs reported in Table 2 together with predictions from CoMFA) and pIC_{50} values ($n = 15$, $r^2 = 0.59$). By excluding from the regression analysis compounds lacking the anchoring lipophilic benzyloxy moieties the correlation significantly improves ($n = 9$, $r^2 = 0.72$). It is worthy of note that, according to the scoring function considered in our case (GRID force field), the BEs are calculated not only in terms of steric, electrostatic or hydrogen bonding interactions, but more realistically taking into account also the enthropic component of the binding, and solvation effects as well.

As a final task of this study, we wanted also to test if QX-GRID was able to discriminate between highly potent and selective reversible MAO Is, such as the two coumarin derivatives in Figure 1 developed in our laboratories. Compound **10**, 7-[(3,4-difluorobenzyl)oxy]-3,4-dimethyl-2*H*-chromen-2-one, had been found to act preferentially on MAO-B with an IC_{50} value in the low-nanomolar range ($pIC_{50} = 8.94$), whereas 3,4-dimethyl-2-oxo-2H-chromen-7-yl 4-nitrobenzenesulfonate (**11**) was the most active reversible MAO-A inhibitor found by us ($pIC_{50} = 7.90$) with negligible inhibition activity toward MAO-B. Due to their so different biological behaviour, depending upon the variation of the moieties at the 7 position of the coumarin nucleus, compounds **10** and **11** were

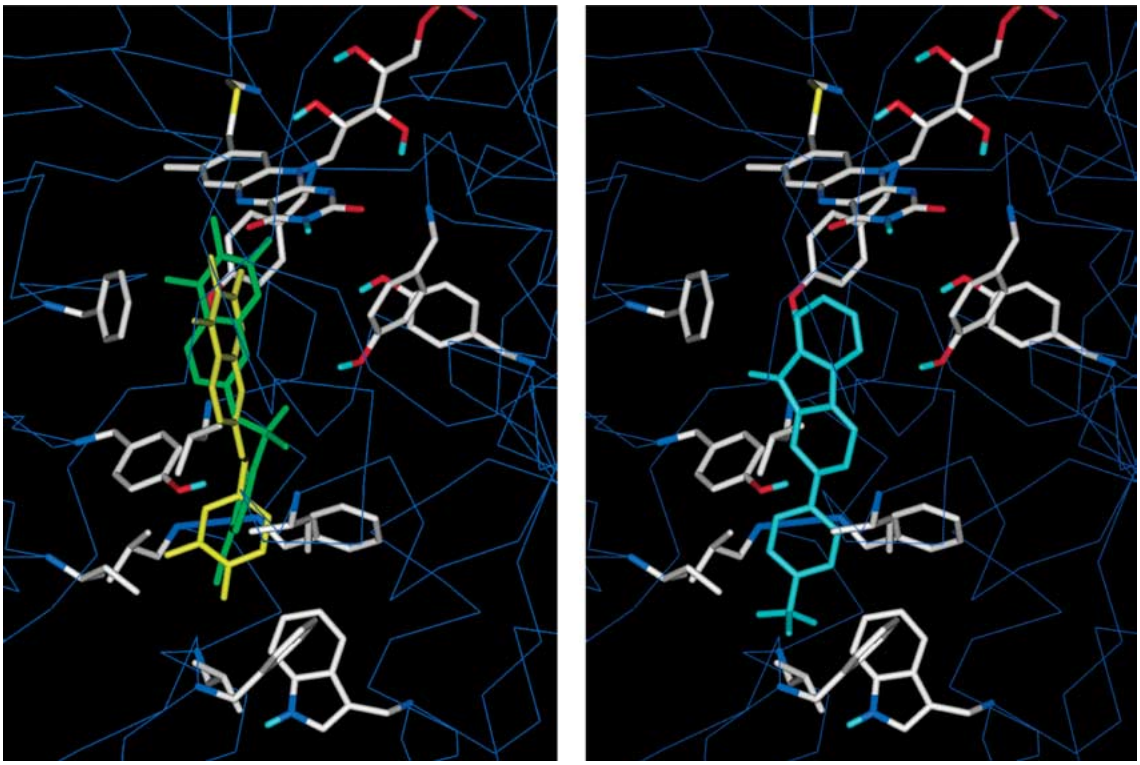

Figure 5. QX/GRID results. Left, coumarin derivatives **10** (MAO-B selective, yellow, BE = −12.34 kcal/mol) and **11** (MAO-A selective, green, BE = −4.33 kcal/mol). Right, indeno-pyridazine derivative **9** (MAO-B selective, cyan, BE = −6.36 kcal/mol).

expected to give proofs of the reliability of the binding models generated using the QX-GRID approach.

The binding mode of the MAO-B I **10**, significantly different from that found for MAO-A I **11** (Figure 5), resembles the binding mode of the diazoheterocyclic derivatives, highlighting once again the role of the hydrophobic interactions between the benzyloxy group and the residues lining the entrance cavity and the interaction of the coumarin 'head' in the substrate cavity. The role of Tyr326 is apparent in such a case; in fact, the affinity of **10**, higher than that of **11**, might also depend upon a more efficient π–π stacking with the aromatic ring of Tyr326. Interestingly, the estimated BEs (−12.39 and −4.33 kcal/mol for **10** and **11**, respectively) properly rank the different measured MAO-B I activity. Once again, it should be pointed out that Tyr326 has been demonstrated as a key residue in controlling the MAOs' selectivity observed in man.

A similar binding mode was obtained as a result of our docking calculation approach as applied to the study of a further good reversible MAO-B inhibitor synthesized in our laboratories, that is 3-[4-(trifluoromethyl)phenyl]-5*H*-indeno[1,2-*c*]pyridazin-5-one (**9**) having a pIC_{50} value of 7.05 (Figure 5).

Conclusions

In an effort to search for novel MAO inhibitors potentially useful as pharmacological agents in the treatment of neurological disorders, including depression and Parkinson's disease, in recent years we discovered new chemical entities, such as 5*H*-indeno[1,2-*c*]pyridazin-5-ones, and coumarin derivatives [34] able to reversibly and selectively inhibit MAO-A and B isoenzymes. In both cases we achieved *ad hoc* rationalizations of the structure-activity relationships by means of both QSAR Hansch-type analysis of the effects of the substituents in some critical positions and CoMFA-based 3D-QSAR studies [14–16].

In order to better understand the mechanism of action at the molecular level and factors of A/B selectivity of the reversible MAO Is, we undertook a 3D-QSAR study on a large dataset of diverse compounds. In this paper we reported on a comprehensive 3D-QSAR model, which integrates different diazo-

heterocyclic compounds (tetrazoles, oxadiazolones, and oxadiazinones) with a set of N-acylhydrazone derivatives, and reveals the array of hydrophobicity, H-bonding and steric hindrance mainly involved in the binding. The 3D-QSAR model agrees quite well with the results from flexible docking calculations, performed by helpfully integrating QXP and GRID computational tools, as applied to a number of selective inhibitors and the X-ray structure of human MAO-B as the receptor target.

As a confirmation of the CoMFA/GOLPE predictions, binding models developed by docking calculations highlighted the role, essential for MAO-B activity and selectivity, of a hydrophobic cavity (the so-called entrance cavity) connecting the surface of the protein to the catalytic cavity, i.e., the primary binding site delimited by Tyr398, Tyr435 and the isoalloxazine ring of FAD, where the aryl diazoheterocycle, substituted by a functionalized (CN, OR) ethyl lateral chain is bound through a network of H-bonds, some of which mediated by water molecules. Taking into account the known MAOs' interspecies differences [35], the correlation trend between the inhibition data measured on rat MAO-B and the energies of the ligand-enzyme complexes calculated with human MAO-B could be considered a satisfactory one. While significant information on the forces controlling the A/B selectivity is expected from our ongoing research on a theoretical 3D model of the MAO-A isoenzyme, obtained by homology building techniques, the results of this study bear evidence of the usefulness of 3D-QSAR and QX-GRID models in the design of new MAO-B inhibitors.

Acknowledgements

This study was financially supported by Italian Ministry for Education Universities and Research (MIUR, Rome, Italy; COFIN 2000). The authors thank Prof. Angelo Carotti (Dipartimento Farmaco-chimico, University of Bari) for his critical comments and helpful suggestions.

References

1. Tripton, K.F., Cell Biochem. Funct., 4 (1986) 79
2. Shih, J.C., Chen, K. and Geha, R.M., J. Neural Transm., 52 (1998) 1
3. Grimsby, J., Lan, N., Neve, R., Chen, K. and Shih, J., J. Neurochem., 55 (1990) 1166
4. Bach, A.W., Lan, N.C., Johnson, D.L., Abell, C.W., Bembenek, M.E., Kwan, S.W., Seeburg, P.H. and Shih, J.C., Proc. Natl. Acad. Sci. U.S.A., 85 (1988) 4934
5. Geha, R.M., Rebrin, I., Chen, K. and Shih, J.C., J. Biol. Chem., 276 (2001) 9877
6. Kochersperger, L.M., Parker, E.L., Siciliano, M., Darlington, G.J. and Denney, R.M., J. Neurosci. Res., 16 (1986) 601
7. Grimsby, J., Chen, K., Wang, L.J., Lan, N.C. and Shih, J.C., Proc. Natl. Acad. Sci. U.S.A., 88 (1991) 3637
8. Fowler, C.J., Callingham, B.A., Mantle, T.J. and Tipton, K.F., Biochem. Pharmacol., 29 (1980) 1177
9. Kalir, A., Sabbagh, A. and Youdim, M.B.H., Brit. J. Pharmacol., 73 (1981) 55
10. Shih, J.C., Chen, K. and Geha, R.M., J. Neural Transm., 52 (1998) 1
11. Wouters, J., Curr. Med. Chem., 5 (1998) 137
12. Sandler, M., Psychol. Med., 11 (1981) 455
13. Foley, P., Gerlach, M., Youdim, M.B.H. and Riederer, P., Parkinsonism & Related Disorders, 6 (2000) 25
14. Kneubuhler, S., Thull, U., Altomare, C., Carta, V., Gaillard, P., Carrupt, P.-A., Carotti, A. and Testa, B., J. Med. Chem., 38 (1995) 3874
15. Altomare, C., Cellamare, S., Summo, L., Catto, M., Carotti, A., Thull, U., Carrupt, P.-A., Testa, B. and Stoeckli-Evans, H., J. Med. Chem., 41 (1998) 3812
16. Gnerre, C., Catto, M., Leonetti, F., Weber, P., Carrupt, P.-A., Altomare, C., Carotti, A. and Testa, B., J. Med. Chem., 43 (2000) 4747
17. Binda, C., Newton-Vinson, P., Hubalek, F., Edmondson, D.E. and Mattevi, A., Nat. Struct. Biol., 9 (2002) 22
18. Lebreton, L., Curet, O., Gueddari, S., Mazouz, F., Bernard, S., Burstein, C. and Milcent, R., J. Med. Chem., 38 (1995) 4786
19. Mazouz, F., Gueddari, S., Burstein, C., Mansuy, D. and Milcent, R., J. Med. Chem., 36 (1993) 1157
20. Mazouz, F., Lebreton, L., Milcent, R. and Burstein, C., Eur. J. Med. Chem., 25 (1990) 659
21. Mazouz, F., Lebreton, L., Milcent, R. and Burstein, C., Eur. J. Med. Chem., 23 (1988) 441
22. Bernard, S., Paillat, C., Oddos, T., Seman, M. and Milcent, R., Eur. J. Med. Chem., 30 (1995) 471
23. McMartin, C. and Bohacek, R.S., J. Comput. Aid.-Mol. Des., 11 (1997) 333
24. Goodford, P.J., J. Med. Chem., 28 (1985) 849
25. Stewart, J.J.P., J. Comput.-Aid. Mol. Des., 4 (1990) 1
26. Wouters, J., Ooms, F., Jegham, S., Koenig, J. J., George, P. and Durant, F., Eur. J. Med. Chem., 32 (1997) 721
27. Ferenczy, G.G., Reynolds , C.A., and Richards, W.G., Eur. J. Comp. Chem., 11 (1990) 159
28. Gaillard, P., Carrupt, P.-A., Testa, B. and Boudon, A., J. Comput. Aid. Mol. Des., 8 (1994) 83
29. Cramer, R.D. III, Patterson, D.E. and Bunce, J.D., J. Am. Chem. Soc., 110 (1988) 5959
30. Baroni, M., Constantino, G., Cruciani, G., Parigi, R. and Clementi, S., Quant. Struct.-Act. Relat., 12 (1993) 9
31. Mohamadi, F., Richards, N.G.J., Guida, W.C., Liskamp, R., Lipton, M., Caufield, C., Chang, G., Hendrickson, T. and Still, W.C., J. Comput. Chem. 11 (1990) 440
32. Wang, R., Lai, L. and Wang, S., J. Comput.-Aid. Mol. Des., 16 (2002) 11
33. Taylor, R.D., Jewsbury, P.J. and Essex, J.W., J. Comput.-Aid. Mol. Des., 16 (2002) 151
34. Carotti, A., Carrieri, A., Chimichi, S., Boccalini, S. M., Cosimelli, B., Gnerre, C., Carotti, A., Carrupt, P.-A., Testa, B., Bioorg. Med. Chem. Lett., 12 (2002) 3551
35. Geha, R.M., Chen, K. and Shih, J.C., J. Neurochem., 75 (2000) 1304